

Nystrom-Type Method in Three-Dimensional Electromagnetic Diffraction by a Finite PEC Rotationally Symmetric Surface

Vitaliy S. Bulygin, *Member, IEEE*, Alexander I. Nosich, *Fellow, IEEE*, and Yuriy V. Gandel, *Senior Member, IEEE*

Abstract—Time-harmonic electromagnetic wave diffraction by a perfectly electrically conducting (PEC) finite rotationally symmetric surface located in free space is investigated. The problem is split to independent azimuth orders and reduced to the sets of coupled hypersingular and singular integral equations (IEs) for the surface current components. These IEs are discretized by the Nystrom-type method of discrete singularities using the interpolation type quadrature formulas. From the solutions of corresponding matrix equations the near- and the far-field patterns are obtained. The presented method has guaranteed convergence for arbitrary not axially symmetric primary field.

Index Terms—Body of revolution (BOR), focusing, interpolation type quadrature formulas, radar cross-section, scattering, singular and hypersingular integral equations.

I. INTRODUCTION

TODAY, efficient development of various devices and systems using electromagnetic waves is unthinkable without preliminary computer-aided design. One of the traditional problems in this area is the analysis of the wave scattering and beamforming by various reflectors. Reflectors are usually thin and therefore can be considered as zero-thickness screens or open surfaces; if made of conventional metals, they can be considered as perfectly electrically conducting (PEC) in the microwave to short-terahertz ranges. However, almost all practically important reflectors are three-dimensional (3-D). Together with the vectorial nature of the Maxwell equations, this means, strictly speaking, that analysis of wave scattering by reflectors cannot be reduced to simplified two-dimensional (2-D) formulations. Still, as the whole idea of a reflector is borrowed from the ray optics, most of reflectors used in practice are large in terms of the wavelength. This circumstance offers a hope that high-frequency approximations, both empiric and grounded, can be useful. Indeed, today the engineering simulations of reflectors are usually done

using geometrical optics and its derivatives, such as geometrical theory of diffraction [1], or physical optics and physical theory of diffraction. The most advanced versions of the latter exploit the very fruitful idea of expanding the fields in terms of Gaussian beams or, better, complex-source-point beams [2], [3]. They are, however, not sufficiently accurate near reflectors and generally fail if the near- and medium-zone environment of reflector is complicated by the presence of subreflectors, radomes, and earth surface. Therefore, the full-wave simulation tools have been, and still are, in demand.

The method of moments (MoM) models based on the electric-field integral equations (IEs) are attractive as these IEs are fully equivalent to the Maxwell-equation problem (provided that the reflector is zero-thickness), satisfy the radiation condition explicitly, and need to mesh only the reflector surface. Among the remarkable earlier MoM versions, one can mention [4]–[6], while the more recent are in [7] and [8]. However, if used in the numerical modeling of 3-D diffraction by an arbitrary PEC open surface, they lead to huge-size matrices that entail large computer resources. Still more important is that their convergence is not uniformly guaranteed, which is caused by the singular character of the IE kernels.

A powerful remedy was developed during the 1980s in the form of the Method of Analytical Regularization (MAR) [9]. MAR is equivalent to a judicious choice of the entire-domain expansion functions in Galerkin MoM. If they are taken as the orthogonal eigenfunctions of the most singular part of the IE operator, projection to them plays the role of a perfect preconditioner [10] and turn the IE into a Fredholm second-kind infinite-matrix equation; the convergence is then guaranteed [9].

The alternative to MAR is the meshless Nystrom-type numerical algorithms having guaranteed convergence and developed recently for 2-D problems [11], [12], [31]. Here, the current density is sought as a product of unknown smooth function and known weight. In either polarization, the weight is chosen in conformity with the edge condition, and the smooth function is approximated with a polynomial of finite order. The convergence is guaranteed due to the properties of the interpolation-type quadrature formulas that take into account both the IE singularities and the weights [13], [14]. Extension of the Nystrom method to arbitrary 3-D reflectors is difficult, however, because it is necessary to satisfy the edge condition analytically and derive interpolation type quadrature formulas for double hypersingular and singular integrals.

Recently, the locally corrected Nystrom (LCN) method has been applied to 2-D and 3-D scattering problems [15]–[17]. The LCN method uses accurate quadrature formulas introduced by

Manuscript received June 09, 2011; revised May 23, 2012; accepted July 02, 2012. Date of publication July 17, 2012; date of current version October 02, 2012. This work was supported in part by the European Science Foundation via the networking programme “Newfocus” and the National Academy of Sciences of Ukraine.

V. S. Bulygin and A. I. Nosich are with the Laboratory of Micro and Nano Optics, Institute of Radio-Physics and Electronics of the National Academy of Sciences of Ukraine, Kharkiv 61085, Ukraine (e-mail: vitaliy_bulygin@yahoo.com; anosich@yahoo.com).

Y. V. Gandel is with the Department of Mathematical Physics and Computational Mathematics, Kharkiv National University, Kharkiv 61077, Ukraine (e-mail: yuriy.v.gandel@univer.kharkov.ua).

Color versions of one or more of the figures in this paper are available online at <http://ieeexplore.ieee.org>.

Digital Object Identifier 10.1109/TAP.2012.2209194

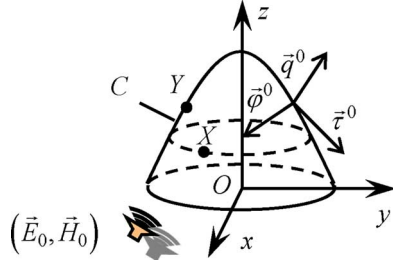


Fig. 1. Generic geometry of a finite PEC surface of rotation.

Stain [18]. At first, the weights for smooth function integration are constructed, and then they are locally corrected near the singularity to obtain an accurate quadrature formula for a singular integral. However, discrete inverse operator existence is not proved, and therefore this method does not have guaranteed convergence.

The axially symmetric PEC reflectors represent a very important subset of possible shapes. One of the first fully 3-D numerical analyses of closed PEC BOR has been done by Andreassen [19]. A more arbitrary case of impedance boundary condition on closed BOR was considered in [20]. Among the works on diffraction by open PEC surfaces of rotation, one should mention the papers [21]–[23]. Because of the analytical manner of taking into account the axial symmetry, authors reduce the 3-D problem to a set of 1-D IEs that significantly lowered the orders of the corresponding matrix equations. However, these advanced versions of MoM use low-order basis functions and still do not have guaranteed convergence.

As for the 3-D MAR-based algorithms, they have been developed so far only for a few rotationally symmetric zero-thickness PEC screens of simple shapes: flat disk [24], finite circular cylinder [25], spherical disk [26], and finite cone [27]. The corresponding numerical results can be considered as reference ones; however, they relate only to the near and far fields of on-axis dipoles and, for flat and spherical disks, to the broadside incidence of plane wave.

In this paper, we consider the diffraction of an arbitrary electromagnetic wave by an arbitrary PEC open surface of rotation. In Section II, we present the formulation of the problem and reduce it to a set of two coupled IEs, one hypersingular and the other singular, for each azimuth order of the surface current components. For the IEs' numerical solution, we develop new interpolation-type quadrature formulas. In Section III, we validate our numerical technique, demonstrate a high rate of convergence, and present numerical results on the monostatic radar cross-section and the near-field focusing for shallow and deep paraboloidal reflectors. Conclusions are summarized in Section IV. The dependence on time is assumed $e^{i\omega t}$ and omitted throughout the paper.

II. DIFFRACTION BY A SURFACE OF ROTATION

A. Problem Formulation

Consider the problem of arbitrary time-harmonic electromagnetic wave (\vec{E}^0, \vec{H}^0) diffraction by a PEC open surface of rotation S located in free space (see Fig. 1). The total electromagnetic field $(\vec{E}^{\text{tot}}, \vec{H}^{\text{tot}})$ is a sum of the incident field (\vec{E}^0, \vec{H}^0)

and the sought-for scattered field (\vec{E}, \vec{H}) . The latter field must satisfy Maxwell equations off S , PEC boundary condition on S , Meixner edge condition at the rim of S , and Sommerfeld radiation condition at infinity.

Choose cylindrical coordinates ρ, φ, z and assume that the surface S is created by the rotation of contour C around the z -axis. Introduce also the curvilinear orthogonal coordinates q, τ, φ in which the surface S has the parameterization

$$S : q = q_0, \tau \in [-1, 1], \varphi \in [0, 2\pi] \quad (1)$$

and cylindrical coordinates are expressed as

$$\rho = \rho(q, \tau), z = z(q, \tau). \quad (2)$$

Here, the Lamé coefficients of the coordinates q, τ, φ are

$$l_q = \sqrt{(\rho'_q)^2 + (z'_q)^2}, l_\tau = \sqrt{(\rho'_\tau)^2 + (z'_\tau)^2}, l_\varphi = \rho$$

and the unit vectors of curvilinear coordinates are $(\vec{q}^0, \vec{\tau}^0, \vec{\varphi}^0)$

$$\vec{\nu}^0 = (\vec{x}^0 \rho'_\nu \cos \varphi + \vec{y}^0 \rho'_\nu \sin \varphi + \vec{z}^0 z'_\nu) / l_\nu, \nu = q, \tau \quad (3)$$

$$\vec{\varphi}^0 = -\vec{x}^0 \sin \varphi + \vec{y}^0 \cos \varphi \quad (4)$$

where $(\vec{x}^0, \vec{y}^0, \vec{z}^0)$ are unit vectors of Cartesian coordinates, and a combination of prime and subscript $\nu = q, \tau$ means partial derivative with respect to the variable $\nu = q, \tau$.

Then, a point located on S has the following cylindrical coordinates: $\rho = \rho(t) = \rho(q_0, t)$, $z = z(t) = z(q_0, t)$. If t is the integration variable, we will use notations like $\rho_0 = \rho_0(t)$, $z_0 = z_0(t)$, $h_\tau = l_\tau(q_0, t)$, and $t \in [-1, 1]$, while for the observation point on S the notations will be $\rho := \rho(\tau)$, $z := z(\tau)$, $\tau \in [-1, 1]$.

B. Hypersingular and Singular Integral Equations

The electric field vector \vec{E} can be expressed in terms of the scalar and vector electromagnetic potentials as

$$\vec{E} = -\text{grad}\Phi - i\omega\vec{A}. \quad (5)$$

The PEC boundary conditions are

$$E_\tau + E_\tau^0|_S = 0, E_\varphi + E_\varphi^0|_S = 0 \quad (6)$$

or, in terms of potentials,

$$\lim_{X \rightarrow Y} [i\omega A_\tau(X) + (1/l_\tau)\partial\Psi/\partial\tau(X)] = E_\tau^0(Y), Y \in S \quad (7)$$

$$\lim_{X \rightarrow Y} [i\omega A_\varphi(X) + (1/\rho)\partial\Psi/\partial\varphi(X)] = E_\varphi^0(Y), Y \in S. \quad (8)$$

As known, the vector potential can be presented as a convolution with the surface current function

$$\vec{A}(Y) = (\mu/4\pi) \int_S \vec{j}(X) e^{-ikL_{XY}} (L_{XY})^{-1} dS_X \quad (9)$$

where L_{XY} is the distance from the observation point Y to the integration point X , and the scalar potential is given by

$$\Psi = (i/\omega\epsilon\mu)\text{div}\vec{A}. \quad (10)$$

The components of the current density and primary field on surface S are represented as Fourier series in azimuth

$$j_\nu(t, \psi) = \sum_{M=-\infty}^{\infty} j_\nu^M(t) e^{iM\psi}, \nu = \tau, \varphi \quad (11)$$

$$E_\nu^0(t, \psi) = \sum_{M=-\infty}^{\infty} E_\nu^{0(M)}(t) e^{iM\psi}, \nu = \tau, \varphi. \quad (12)$$

As shown in [28], the Fourier series of the scalar and vector potentials have the form

$$A_\nu(q, \tau, \varphi) = \sum_{M=-\infty}^{\infty} A_\nu^M(q, \tau) e^{iM\varphi}, \nu = \tau, \varphi \quad (13)$$

$$\Psi(q, \tau, \varphi) = \sum_{M=-\infty}^{\infty} \Psi^M(q, \tau) e^{iM\varphi} \quad (14)$$

where

$$A_\tau^M(q, \tau) = \mu/(4\pi l_\tau) \int_{-1}^1 [j_\tau^M(t) \rho_0 (z' z'_0 S_M + \rho' \rho'_0 S_M^+) - j_\varphi^M(t) \rho_0 h_\tau \rho' S_M^-] dt \quad (15)$$

$$A_\varphi^M(q, \tau) = (\mu/4\pi) \int_{-1}^1 [j_\tau^M(t) \rho_0 \rho'_0 S_M^- + j_\varphi^M(t) \rho_0 h_\tau S_M^+] dt \quad (16)$$

$$\Psi^M(q, \tau) = (-i/4\pi k) Z \int_{-1}^1 \left[j_\tau^M(t) \rho_0 \frac{\partial S_M}{\partial t} - iM j_\varphi^M(t) h_\tau S_M \right] dt \quad (17)$$

$$S_M(q, \tau, t) = S_M = \int_{-1}^1 \cos(M\psi) (e^{-ikL}/L) d\psi \quad (18)$$

$$L = \sqrt{\rho^2 + \rho_0^2 - 2\rho\rho_0 \cos\psi + (z - z_0)^2}. \quad (19)$$

Introduce new unknown smooth functions $u^M(t)$ and $w^M(t)$ in conformity with the edge condition as

$$j_\tau^M(t) \rho(t) = u^M(t) \sqrt{1-t^2}, j_\varphi^M(t) h_\tau(t) = w^M(t) / \sqrt{1-t^2}. \quad (20)$$

Thus, in (7) and (8), $\lim_{X \rightarrow Y}$ equals $\lim_{q \rightarrow q_0}$ since the point belongs to the surface S if $q = q_0$. If we substitute (9)–(15) into (7) and (8), then we obtain a set of equations with 1-D integrals with the function $S_M(q, \tau, t)$ and its first and second derivatives in the kernels. As $S_M(q_0, \tau, t) \sim (-2/\rho) \ln|\tau-t|$ (see [28]), one cannot move the limit to the integrands of (7) and (8), because of non-integrable singularities $O[(\tau-t)^{-2}]$.

Introduce the following integral operators [13], [14]:

- hypersingular integral operator understood in the sense of Hadamard finite part,

$$(Au)(\tau) = (1/\pi) \int_{-1}^1 u(t) \sqrt{1-t^2}/(\tau-t)^2 dt; \quad (21)$$

- singular integral operators with different weights,

$$(\Gamma u)(\tau) = (1/\pi) \int_{-1}^1 u(t) / [\sqrt{1-t^2} \cdot (\tau-t)] dt \quad (22)$$

$$(\Gamma^{-1}u)(\tau) = (1/\pi) \int_{-1}^1 u(t) \sqrt{1-t^2}/(\tau-t) dt \quad (23)$$

- integral operators with logarithmic kernels,

$$(L^I u)(\tau) = (1/\pi) \int_{-1}^1 \ln|\tau-t| u(t) \sqrt{1-t^2} dt \quad (24)$$

$$(L^{II} u)(\tau) = (1/\pi) \int_{-1}^1 \ln|\tau-t| u(t) / \sqrt{1-t^2} dt \quad (25)$$

- and integral operators with smooth kernels and weights,

$$(K^I u)(\tau) = (1/\pi) \int_{-1}^1 K(\tau, t) u(t) \sqrt{1-t^2} dt \quad (26)$$

$$(K^{II} u)(\tau) = (1/\pi) \int_{-1}^1 K(\tau, t) u(t) / \sqrt{1-t^2} dt. \quad (27)$$

We will denote the integral operators with smooth kernels (26) and (27) and their kernels using similar symbols.

If we take a limit in (7) and (8) using the expressions for the vector and scalar potentials (13)–(17), then we obtain a set of two coupled hypersingular and singular integral equations (HSIE and SIE) with varying coefficients,

$$\begin{pmatrix} a_{11}A + b_{11}\Gamma^{-1} + c_{11}^M L^I + K_{11}^{M(I)} & b_{12}^M \Gamma + c_{12}^M L^{II} + K_{12}^{M(II)} \\ b_{21}^M \Gamma^{-1} + c_{21}^M L^I + K_{21}^{M(I)} & c_{22}^M L^{II} + K_{22}^{M(II)} \end{pmatrix} \cdot \begin{pmatrix} u^M(\tau) \\ w^M(\tau) \end{pmatrix} = \begin{pmatrix} 4ik\rho^3 E_\tau^{0(M)}(\tau) h_\tau(\tau) / Z \\ 4ik\rho^3 E_\varphi^{0(M)}(\tau) / Z \end{pmatrix} \quad (28)$$

where $M = 0, \pm 1, \pm 2, \dots$, and the varying coefficients are

$$a_{11}(\tau) = -2\rho^2, b_{11}(\tau) = -\rho' \rho \quad (29)$$

$$c_{11}^M(\tau) = (k^2 \rho^2 + M^2)(\rho'^2 + z'^2) - (z'^2 + 3\rho'^2)/4 \quad (30)$$

$$b_{12}^M(\tau) = 2iM\rho^2, c_{12}^M(\tau) = -iM\rho'\rho, b_{21}^M(\tau) = 2iM\rho \quad (31)$$

$$c_{21}^M(\tau) = iM\rho', c_{22}^M(\tau) = -2M^2\rho + 2k^2\rho^3 \quad (32)$$

while the smooth kernels are

$$K_{11}^M(\tau, t) = \rho^3 [\partial^2 S_M / \partial t \partial \tau - k^2 (\rho'_0 \rho' S_M^+ + z'_0 z' S_M)] - a_{11}(\tau) / (\tau-t)^2 - b_{11}(\tau) / (\tau-t) - c_{11}^M(\tau) \ln|\tau-t| \quad (33)$$

$$K_{12}^M(\tau, t) = \rho^3 [k^2 \rho_0 \rho' S_M^- - iM \cdot \partial S_M / \partial \tau] - b_{12}^M(\tau) / (\tau-t) - c_{12}^M(\tau) \ln|\tau-t| \quad (34)$$

$$K_{21}^M(\tau, t) = \rho^3 [(iM/\rho) \partial S_M / \partial t - k^2 \rho'_0 S_M^-] - b_{21}^M(\tau) / (\tau-t) - c_{21}^M(\tau) \ln|\tau-t| \quad (35)$$

$$K_{22}^M(\tau, t) = \rho^3 [(M^2/\rho) S_M - k^2 \rho_0 S_M^+] - c_{22}^M(\tau) \ln|\tau-t|. \quad (36)$$

and shorthand notations $S_M^+ = (S_{M+1} + S_{M-1})/2$, $S_M^- = (S_{M+1} - S_{M-1})/2i$ are used.

C. Discretization of IEs

We use the following interpolation type quadrature formulas [12]–[14], [31] for discretization of HSIE and SIE (28):

- quadrature formulas for a hypersingular integral,

$$Au_{n-2}(t_{0l}^n) = \sum_{k=0}^{n-2} A_{l,k} u_{n-2}(t_{0k}^n), \quad A_{kk} = -n/2$$

$$A_{l,k} = [1 - (-1)^{l+k}] \left(1 - (t_{0k}^n)^2\right) / \left[n \cdot (t_{0l}^n - t_{0k}^n)^2\right]$$

$$l \neq k; \quad (37)$$

- quadrature formulas for singular integrals,

$$\Gamma^{-1} u_{n-2}(t_{0l}^n) = \sum_{k=0}^{n-2} \Gamma_{l,k}^{-1(I)} u_{n-2}(t_{0k}^n), \quad \Gamma_{k,k}^{-1(I)} = 0$$

$$\Gamma_{l,k}^{-1(I)} = [1 - (-1)^{l+k}] \left(1 - (t_{0k}^n)^2\right) / [n \cdot (t_{0l}^n - t_{0k}^n)]$$

$$l \neq k \quad (38)$$

$$\Gamma^{-1} u_{n-2}(t_l^n) = \sum_{k=0}^{n-2} \Gamma_{l,k}^{-1(II)} u_{n-2}(t_{0k}^n)$$

$$\Gamma_{l,k}^{-1(II)} = [1 - (t_{0k}^n)^2] / [(t_l^n - t_{0k}^n) \cdot n] \quad (39)$$

$$\Gamma u_{n-2}(t_{0l}^n) = \sum_{k=0}^{n-1} \Gamma_{l,k} u_{n-2}(t_k^n),$$

$$\Gamma_{l,k} = 1 / [(t_{0l}^n - t_k^n) \cdot n] \quad (40)$$

- quadrature formulas for integrals with logarithm kernels,

$$L^I u_{n-2}(\tau) = \sum_{m=0}^{n-2} L_k^I(\tau) u_{n-2}(t_{0k}^n)$$

$$L_k^I(\tau) = - \left[1 - (t_{0k}^n)^2\right] \left[\ln 2 + 2 \sum_{p=1}^{n-1} T_p(t_{0k}^n) T_p(\tau) / p \right. \\ \left. + (-1)^j T_n(\tau) / n \right] / n \quad (41)$$

$$L^{II} u_{n-2}(\tau) = \sum_{k=0}^{n-1} L_k^{II}(\tau) u_{n-2}(t_k^n)$$

$$L_k^{II}(\tau) = \left[\ln 2 + 2 \sum_{p=1}^{n-1} T_p(t_k^n) T_p(\tau) / p \right] / n \quad (42)$$

- and quadrature formulas for integrals with smooth kernels,

$$K^I u_{n-2}(\tau) = \sum_{k=0}^{n-2} K_{l,1}^{k(I)}(\tau) u_{n-2}(t_{0k}^n)$$

$$K_{l,1}^{k(I)}(\tau) = K_{l,1}(\tau, t_{0k}^n) \left(1 - (t_{0k}^n)^2\right) / n, \quad l = 1, 2 \quad (43)$$

$$K^{(II)} u_{n-1}(\tau) = \sum_{k=0}^{n-1} K_{m,2}^{k(II)}(\tau) u_{n-1}(t_k^n)$$

$$K_{m,2}^{k(II)}(\tau) = K_{m,2}(\tau, t_k^n) / n, \quad m = 1, 2. \quad (44)$$

On satisfying the first IE of (28) in the zeros of the second-kind Chebyshev polynomial $\{t_{0j}^n\}_{j=0}^{n-2} = \{\cos(j + 1)\pi/n\}_{j=0}^{n-2}$ and the second IE in the zeros of the first-kind polynomial $\{t_k^n\}_{k=0}^{n-1} = \{\cos(2k + 1)\pi/(2n)\}_{k=0}^{n-1}$ and using the

quadrature formulas (37)–(44), we obtain discrete counterpart of (28),

$$C^M x^M = b^M, \quad M = 0, \pm 1, \pm 2, \dots \quad (45)$$

$$x^M = \left(\{u_{n-2}^M(t_{0k_1}^n)\}_{k_1=0}^{n-2}, \{w_{n-1}^M(t_{k_2}^n)\}_{k_2=0}^{n-1} \right)^T \quad (46)$$

$$b^M = \left(\{g_{1,n-2}^M(t_{0l_1}^n)\}_{l_1=0}^{n-2}, \{g_{1,n-1}^M(t_{l_2}^n)\}_{l_2=0}^{n-1} \right)^T \quad (47)$$

$$C^M = \begin{pmatrix} C^{(M)11} & C^{(M)12} \\ C^{(M)21} & C^{(M)22} \end{pmatrix} \quad (48)$$

$$C^{(M)11} = \left\{ C_{l_1, k_1}^{(M)11} \right\}_{l_1, k_1=0}^{n-2}$$

$$C^{(M)12} = \left\{ C_{l_1, k_2}^{(M)12} \right\}_{l_1=0, k_2=0}^{n-2, n-1}$$

$$C^{(M)21} = \left\{ C_{l_2, k_1}^{(M)21} \right\}_{l_2=0, k_1=0}^{n-1, n-2}$$

$$C^{(M)22} = \left\{ C_{l_2, k_2}^{(M)22} \right\}_{l_2, k_2=0}^{n-1} \quad (49)$$

$$C_{l_1, k_1}^{(M)11} = a_{11}(t_{0l_1}^n) A_{l_1, k_1} + b_{11}(t_{0l_1}^n) \Gamma_{l_1, k_1}^{-1(I)}$$

$$+ c_{11}^M(t_{0l_1}^n) L_{k_1}^I(t_{0l_1}^n) + K_{1,1}^{k_1(I)}(t_{0l_1}^n) \quad (50)$$

$$C_{l_1, k_2}^{(M)12} = b_{12}^M(t_{0l_1}^n) \Gamma_{l_1, k_2} + c_{12}^M(t_{0l_1}^n) L_{k_2}^{II}(t_{0l_1}^n) + K_{1,2}^{k_2(II)}(t_{0l_1}^n) \quad (51)$$

$$C_{l_2, k_1}^{(M)21} = b_{21}^M(t_{l_2}^n) \Gamma_{l_2, k_1}^{-1(II)} + c_{21}^M(t_{l_2}^n) L_{k_1}^I(t_{l_2}^n)$$

$$+ K_{2,1}^{k_1(I)}(t_{l_2}^n) \quad (52)$$

$$C_{l_2, k_2}^{(M)22} = c_{22}^M(t_{l_2}^n) L_{k_2}^{II}(t_{l_2}^n) + K_{2,2}^{k_2(II)}(t_{l_2}^n) \quad (53)$$

where $u_{n-2}^M(t_0)$ and $w_{n-1}^M(t)$ denote the polynomials of the degrees $n - 2$ and $n - 1$, respectively.

Using the technique described in [13] and [14], we have proven that the set (28) has a unique solution in the corresponding Hilbert spaces for each value of the parameter M . If the parameterization functions $\rho_0(t)$, $z_0(t)$ are polynomials, then approximate solutions $u_{n-2}^M(t_0)$ and $w_{n-1}^M(t)$ converge to the exact solution of (28) for $n \rightarrow \infty$ with the rate of convergence $1/n$.

D. Near-Field and Far-Field Patterns

On substituting the expressions (13)–(17) into (6), we obtain the expressions for the electrical field components via the solutions $u_{n-2}^M(t_0)$ and $w_{n-1}^M(t)$ of the set (28),

$$E_\nu(\rho, z, \varphi) = \sum_{M=-\infty}^{\infty} E_\nu^M(\rho, z) e^{iM\varphi}, \quad \nu = \rho, \varphi, z \quad (54)$$

$$E_\nu^M(\rho, z) = (iZ/4\pi k) \left[\int_{-1}^1 Q_{\nu\tau}^M(\rho, z, t) u^M(t) \sqrt{1-t^2} dt \right. \\ \left. + \int_{-1}^1 Q_{\nu\varphi}^M(\rho, z, t) w^M(t) / \sqrt{1-t^2} dt \right]$$

$$\nu = \rho, \varphi, z \quad (55)$$

$$Q_{\rho\tau}^M = \frac{\partial^2 S_M}{\partial \rho \partial t} - k^2 \rho_0' S_M^+$$

$$Q_{\rho\varphi}^M = \rho_0 k^2 S_M^- - iM \frac{\partial S_M}{\partial \rho} \quad (56)$$

$$\begin{aligned} Q_{\varphi\tau}^M &= \frac{iM}{\rho} \frac{\partial S_M}{\partial t} - k^2 \rho'_0 S_M^-, \\ Q_{\varphi\varphi}^M &= \frac{M^2}{\rho} S_M - k^2 \rho_0 S_M^+ \end{aligned} \quad (57)$$

$$\begin{aligned} Q_{z\tau}^M &= \partial^2 S_M / \partial z \partial t - k^2 z'_0 S_M \\ Q_{z\varphi}^M &= (-iM) \partial S_M / \partial z. \end{aligned} \quad (58)$$

The far-field scattering pattern components are defined as

$$F_\eta(\theta, \varphi) = \lim_{R \rightarrow \infty} E_\eta(R, \theta, \varphi) R e^{ikR}, \eta = \theta, \varphi. \quad (59)$$

Using (54)–(57) and the following limit expression:

$$\begin{aligned} f^M(\theta, t) &= \lim_{R \rightarrow \infty} S_M(R, \theta, t) R e^{ikR} \\ &= i^M 2\pi e^{ikz_0 \cos \theta} J_M(k\rho_0 \sin \theta) \end{aligned} \quad (60)$$

we obtain the far-field scattering pattern components as

$$F_\nu(\theta, \varphi) = \sum_{M=-\infty}^{+\infty} e^{iM\varphi} F_\nu^M(\theta), \nu = \theta, \varphi \quad (61)$$

$$F_\nu^M(\theta) = (iZ/4\pi k) \left[\int_{-1}^1 U_{\nu\tau}^M(\theta, t) u^M(t) \sqrt{1-t^2} dt + \int_{-1}^1 U_{\nu\varphi}^M(\theta, t) w^M(t) (1-t^2)^{-1/2} dt \right] \quad (62)$$

$$U_{\varphi\tau}^M = (-k^2 \rho'_0 / 2i) (f^{M+1} - f^{M-1}) \quad (63)$$

$$U_{\varphi\varphi}^M = (-k^2 \rho_0 / 2) (f^{M+1} + f^{M-1}) \quad (64)$$

$$U_{\theta\tau}^M = k^2 [z'_0 f^M \sin \theta - \rho'_0 \cos \theta (f^{M+1} + f^{M-1}) / 2] \quad (65)$$

$$U_{\theta\varphi}^M(\theta, t) = k^2 \rho_0 \cos \theta (f^{M+1} - f^{M-1}) / 2i. \quad (66)$$

Introduce the vector far-field scattering pattern as

$$\vec{F}^{\text{tot}}(\theta, \varphi) = \vec{F}(\theta, \varphi) + \vec{F}^0(\theta, \varphi) \quad (67)$$

where $\vec{F}^0(\theta, \varphi)$ is the incident field pattern, and denote

$$F(\theta, \varphi) = \sqrt{|F_\theta(\theta, \varphi)|^2 + |F_\varphi(\theta, \varphi)|^2} \quad (68)$$

Using quadrature formulas (43) and (44), we obtain the following formulas for the electric field and the far-field scattering patterns of the M th azimuthal order, respectively:

$$\begin{aligned} E_\nu^{(n)M}(\rho, z) &= (iZ/4k) \left[\sum_{k_2=0}^{n-1} Q_{\nu\varphi}^M(\rho, z, t_{k_2}^n) w_{n-1}^M(t_{k_2}^n) + \sum_{k_1=0}^{n-2} Q_{\nu\tau}^M(\rho, z, t_{0k_1}^n) u_{n-2}^M(t_{0k_1}^n) \right] \\ &\times \left[1 - (t_{0k_1}^n)^2 \right], \nu = \rho, \varphi, z \end{aligned} \quad (69)$$

$$\begin{aligned} F_\eta^{(n)M}(\theta) &= (iZ/4k) \left[\sum_{k_2=0}^{n-1} U_{\eta\varphi}^M(\theta, t_{k_2}^n) w_{n-1}^M(t_{k_2}^n) + \sum_{k_1=0}^{n-2} U_{\eta\tau}^M(\theta, t_{0k_1}^n) u_{n-2}^M(t_{0k_1}^n) \right] \\ &\times \left[1 - (t_{0k_1}^n)^2 \right], \eta = \theta, \varphi. \end{aligned} \quad (70)$$

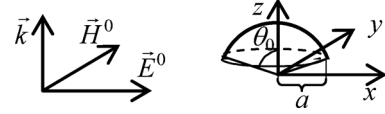


Fig. 2. Spherical disk illuminated by the normally incident plane wave (NIPW).

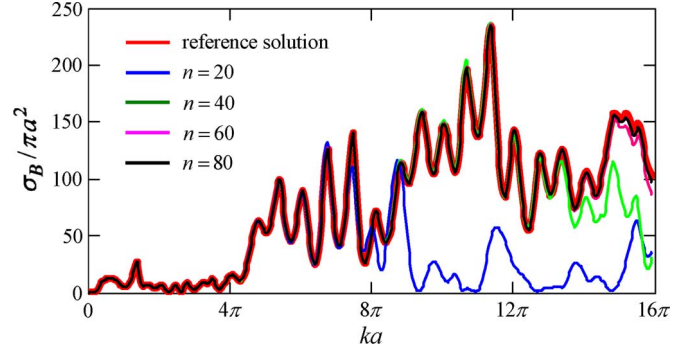


Fig. 3. Normalized monostatic RCS of a hemispherical disk calculated using [26] with accuracy 10^{-6} (reference solution) and our algorithm with interpolation orders $n = 20, 40, 60, 80$ as a function of normalized frequency.

III. VALIDATION

Consider a PEC spherically curved disk of the radius a and angular width $2\theta_0$ illuminated by the plane wave having electric field $\vec{E}^0 = Z(e^{-ikz}, 0, 0)$ and propagating parallel to the rotation axis, as shown in Fig. 2.

In this case, the incident field has components given by

$$E_\tau^0 = e^{-ikz} \rho' \cdot \cos \varphi / h_\tau, E_\varphi^0 = -e^{-ikz} \sin \varphi. \quad (71)$$

From (71), it is obvious that if $M \neq \pm 1$, then $E_{\tau,\varphi}^{0(M)} = 0$ and $E_\tau^{0(1)} = E_\tau^{0(-1)}$, $E_\varphi^{0(1)} = -E_\varphi^{0(-1)}$. This leads to the conclusion that $u^M = w^M = 0$ if $M \neq \pm 1$ and $u^1 = u^{-1}$, $w^1 = -w^{-1}$, hence $F_\theta(\theta, \varphi) = 2F_\theta^1(\theta) \cos \varphi$ and $F_\varphi(\theta, \varphi) = 2iF_\varphi^1(\theta) \sin \varphi$.

In [26], this problem was reduced, using MAR, to the Fredholm second-kind matrix equation. The corresponding algorithm has guaranteed convergence and, if the matrix size is adapted to the parameter ka , provides results with a desired accuracy up to machine precision. We have computed, using this algorithm with uniform accuracy 10^{-6} , the monostatic radar cross-section (RCS), $\sigma_B = 4\pi |F(\pi, 0)|^2$, of a hemi-spherical disk ($\theta_0 = \pi/2$) for ka varying from 0 to 50—see Fig. 3. This curve is shown as a reference solution.

Four other curves correspond to RCS calculated using the method proposed here, with different values of the interpolation order n . One can see that, for a graphical coincidence of results, it is necessary to take $n \geq k \cdot \pi a / 2 + 5$, where πa is the length of the reflector cross-section contour.

In Fig. 4(a), we show the error in the far-field scattering pattern $\vec{F}(\theta, \varphi)$ for several values of n . In addition, the actual rate of convergence is demonstrated in Fig. 4(b) where the reference values of RCS as computed by [26] are $\sigma_B / \pi a^2 = 53.7309674$ and 144.551412 at $ka = 5\pi$ and 10π , respectively.

A test of the numerical stability of our algorithm can be performed if we take the functions $u(t) = u_{n-2}(t)$ and $w(t) =$

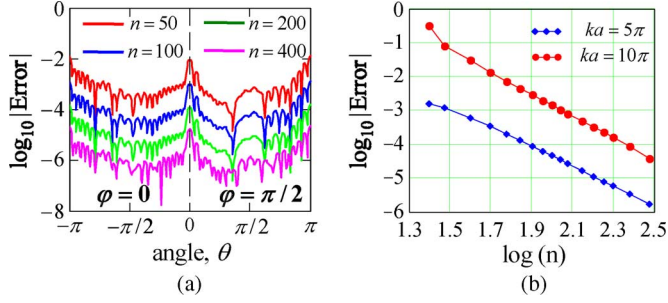


Fig. 4. The errors in the far-field patterns in two principal planes for $ka = 10\pi$ (a) and the error in the monostatic RCS as a function of $\log(n)$ for $ka = 5\pi$, 10π (b), $\theta_0 = 90^\circ$.

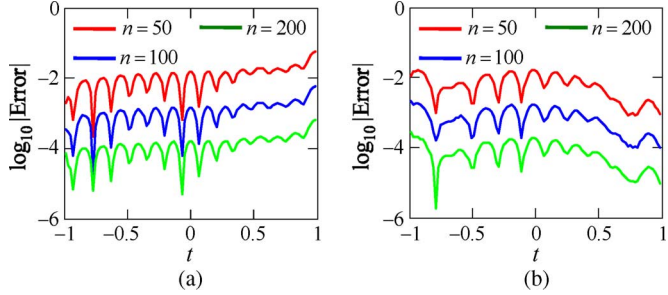


Fig. 5. The errors in the functions (a) $u(t)$ and (b) $w(t)$ for $ka = 10\pi$, $\theta_0 = 90^\circ$ and varying n . The reference solutions are those for $n = 400$.

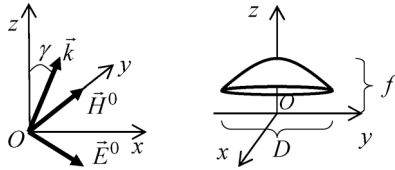


Fig. 6. Paraboloidal reflector illuminated by electromagnetic plane wave.

$w_{n-1}(t)$ computed for $n = 400$, $ka = 10\pi$, $\theta_0 = 90^\circ$ as a reference, and compare them to the same functions computed with smaller values of n . This comparison is shown in Fig. 5.

IV. PARABOLOID ILLUMINATED BY A PLANE WAVE

A. Monostatic Radar Cross Section

Consider a paraboloidal reflector with the focal distance f and the diameter D (see Fig. 6) illuminated by the plane wave having electric field

$$\vec{E}^0(\rho, \varphi, z) = \vec{m}e^{-i(\vec{k}, \vec{R})} \quad (72)$$

where $\vec{m} = (\cos \gamma, 0, -\sin \gamma)$, $\vec{k} = k(\sin \gamma, 0, \cos \gamma)$, and $\vec{R} = (\rho \cos \varphi, \rho \sin \varphi, z)$. Using (3) and (4), we obtain

$$E_\varphi^{0(M)} = -(Z/2i)(-i)^{M-1} [J_{M-1}(T) + J_{M+1}(T)] \times \cos \gamma e^{-ikz \cos \gamma} \quad (73)$$

$$E_\tau^{0(M)} = (Z/2)(-i)^M \{ (i\rho'_\tau \cos \gamma [J_{M-1}(T) - J_{M+1}(T)] - 2z'_\tau \sin \gamma J_M(T) \} e^{-ikz \cos \gamma} / l_\tau$$

$$T = k\rho \sin \gamma. \quad (74)$$

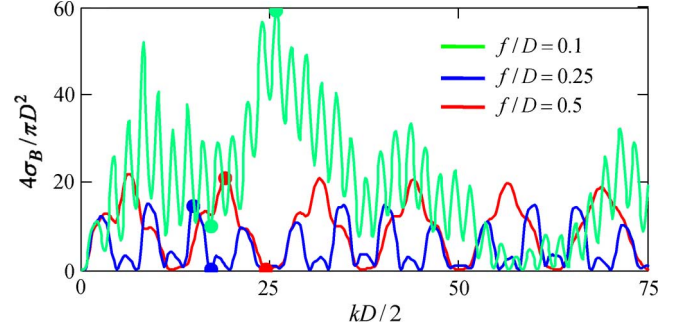


Fig. 7. Paraboloidal reflector normalized monostatic RCS as a function of the normalized frequency in the case of the normal incidence ($\gamma = 0$).

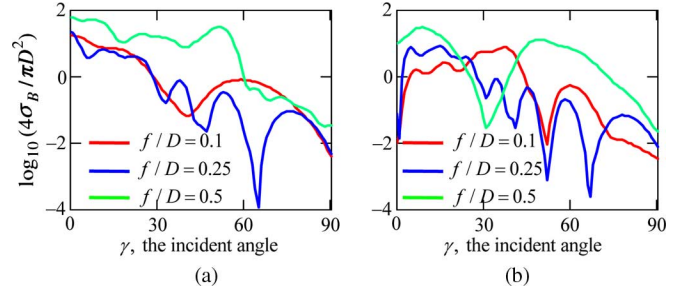


Fig. 8. RCS as a function of incidence angle γ in the (a) local maxima $kD/2 = 25.88, 14.9, 19.2$ and (b) minima $kD/2 = 17.2, 17.2, 24.6$.

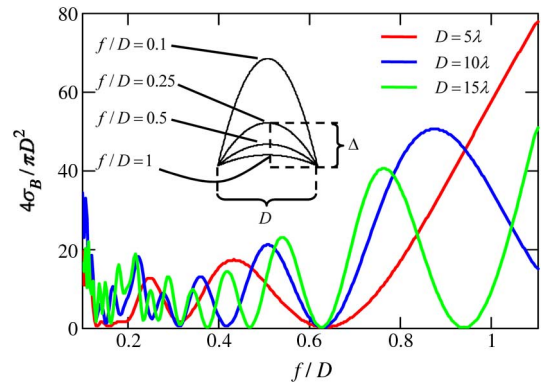


Fig. 9. Paraboloidal reflector normalized monostatic RCS as a function of the f/D in the case of $D = 5\lambda, 10\lambda, 15\lambda$, $\gamma = 0$.

In Fig. 7, we show the variation of the monostatic RCS, $\sigma_B = 4\pi|F(\pi + \gamma, 0)|^2$, versus the normalized frequency for the normal incidence ($\gamma = 0$) and three values of f/D .

Note that the quasi-period of RCS oscillations, in frequency, for reflectors with $f/D = 0.25$ and 0.1 is two and five times smaller, respectively, than for $f/D = 0.5$. These oscillations are caused by the interference of the field reflected by the paraboloid bottom with the field reflected by its rim.

The variation of the monostatic RCS with the plane wave incidence angle γ in the marked in Fig. 7 local maxima and minima for the considered three reflectors is shown in Fig. 8.

In Fig. 9, we show σ_B as a function of f/D in the case of normal incidence and three different values of reflector diameter D . Note that if D is fixed and f/D value increases, then the paraboloid depth $\Delta = D^2/16f$ decreases. As one can see,

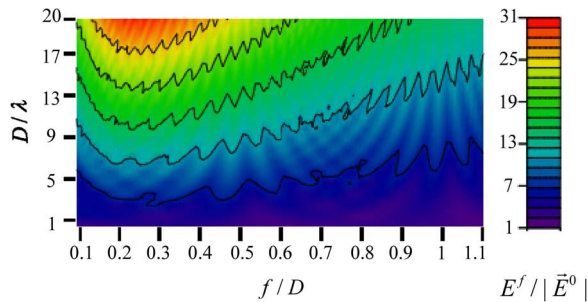


Fig. 10. The equal-value curves for the total electric field in the geometric focus of paraboloidal reflector as a function of f/D and D/λ .

the RCS of paraboloid under the broadside illumination drops several orders of magnitude at certain frequencies.

Based on the ray tracing, this effect was explained in [29] and linked to the paraboloid depth being an integer $\lambda/2$ multiple.

This condition means that $kD/2 = 8\pi m(f/D)$ and $f/D = D/(8\lambda m)$, $m = 1, 2, 3 \dots$, which is in good agreement with the minima on the curves in Figs. 7 and 9. The new point is that the RCS of paraboloid almost vanishes at these values of its depth only for shallow paraboloids ($f/D > 0.25$). For deeper paraboloids, this rule is not true both in terms of the RCS minima location and their values. Thus, geometrical optics fails for deep paraboloids even if they are large.

B. Focusing Ability

The field in the geometrical focus is of particular interest as a receiving horn is normally placed there. Its magnitude is shown in Fig. 10 as a function of f/D and D/λ . One can see that if the frequency and the dish diameter are fixed, then the largest in-focus electric field is achieved for a shallow dish with $f/D = 0.25$. This is rigorous proof of the well-known engineering fact: deep reflectors have no merits. The optimal value of f/D corresponds to the reflector whose geometrical focus lies in the same plane as its rim (see [30] and [32]).

In Fig. 11, we show the total electric-field magnitude patterns in two principal planes near an optimal paraboloidal reflector with $f/D = 0.25$ and $D = 20\lambda$, illuminated by the normally incident plane wave (NIPW). A zoom of the field near the geometrical focus is also shown in the top. Note that here the maximum value of $|\vec{E}^{\text{tot}}|/|\vec{E}^0|$ is 31.61 found at $(0, 0, 0.11\lambda)$ and not in the geometrical focus $(0,0,0)$.

In Fig. 12, the total electric field magnitude is shown in the near-zone of the deep paraboloidal reflector with $f/D = 0.1$, $D = 20\lambda$ illuminated by the NIPW. The maximum value of the $|\vec{E}^{\text{tot}}|$ in Fig. 11 is 29.63 at the point $(0.3\lambda, 0, 0)$, which does not coincide with the geometric focus $(0,0,0)$.

In the case of inclined incidence ($\gamma \neq 0$) all primary-field azimuth harmonics are non zero however their contribution decays with $|M| \rightarrow \infty$. We have found that to obtain results with graphical accuracy, one can truncate the azimuth series at the order M_0 , for which $|4ik\rho^3 E_\varphi^{0(M_0)}(\tau)/Z| < \varepsilon$ and $|4ik\rho^3 E_\tau^{0(M_0)}(\tau)h_\tau(\tau)/Z| < \varepsilon$ with $\varepsilon = 10^{-6}$.

In Fig. 13, we show the total electric field magnitude in the near-zone of a deep paraboloidal reflector with $f/D = 0.1$,

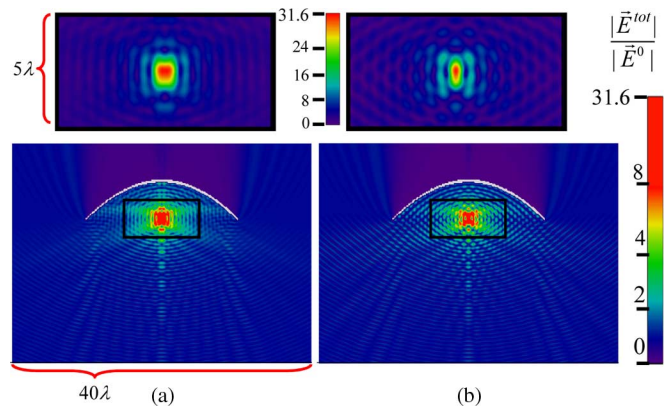


Fig. 11. The near fields of the paraboloidal reflector with $f/D = 0.25$, $D = 20\lambda$ illuminated by the NIPW, in (a) the E-plane and (b) the H-plane.

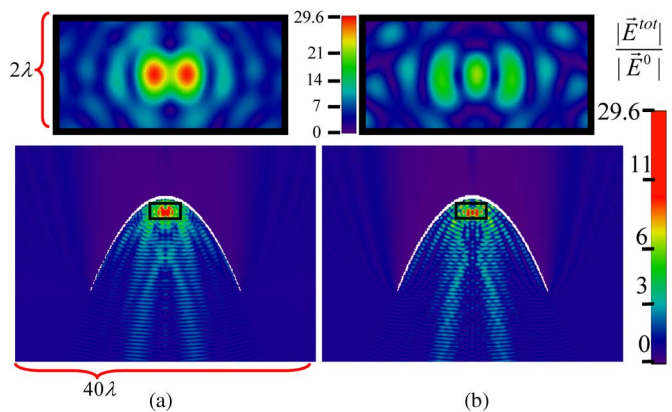


Fig. 12. The near fields of the paraboloidal reflector with $f/D = 0.1$, $D = 20\lambda$ illuminated by the NIPW, in (a) the E-plane and (b) the H-plane.

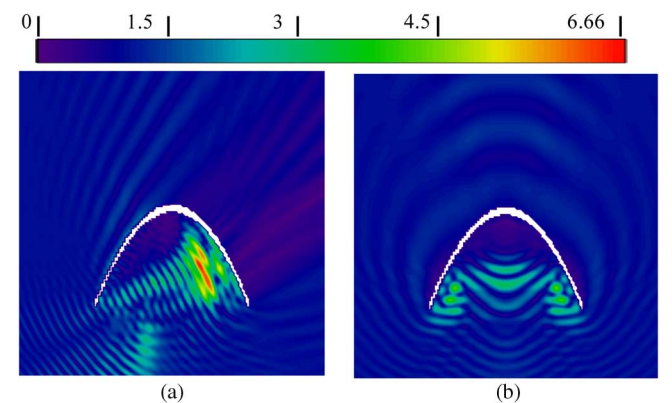


Fig. 13. The near fields of a deep paraboloidal reflector with $f/D = 0.1$, $D = 10\lambda$ illuminated by the plane wave under $\gamma = 50^\circ$ incidence, in (a) the E-plane and (b) the H-plane.

$D = 10\lambda$ illuminated by the plane wave under the $\gamma = 50^\circ$ incidence. In this case it is necessary to take $M_0 = 34$ harmonics.

As one can see, here a strong local maximum is formed near to the directly illuminated inner part of the reflector, and the local near field resembles a standing plane wave. This indicates to the stronger back-reflection by that part of the paraboloid at this angle of incidence. Such a behavior is consistent with the enhanced RCS at the same $\gamma = 50^\circ$, as shown in Fig. 8(a).

V. CONCLUSION

Summarizing, we have presented a convergent and efficient meshless numerical method for the analysis of an arbitrary PEC rotationally symmetric screen illuminated by an arbitrary electromagnetic field. Unlike [15]–[18], in the present paper, we separate integrals with simple hypersingular, singular, and logarithm kernels analytically and use exact interpolation type quadrature formulas to approximate them.

The developed method is especially economic if the incident field consists of finite number of Fourier azimuth harmonics. For example, in the case of illumination by a plane electromagnetic wave propagating parallel to the axis of rotation, it is necessary to solve only one pair of coupled 1-D HSIE and SIEs. The method has high rate of convergence: three correct digits in the far-field analysis can be found after solving as small matrix as of the order $n \geq kL + 5$, where L is the length of the reflector cross-section contour. As a consequence, the analysis of a $50\text{-}\lambda$ reflector takes minutes on a moderate desktop computer.

The method validation has been done using plane electromagnetic wave diffraction by a PEC spherical disk. The comparison of our results for the monostatic RCS with those generated by the size-adapted MAR-based algorithm of [26] has shown perfect agreement within a desired number of digits. The analysis of the near fields has also demonstrated agreement with the patterns published in [30] and [32].

Using our algorithm, we have obtained the numerical data concerning the variation of the monostatic RCS of shallow and deep paraboloidal reflectors with the wavelength, focal distance, and angle of the plane wave incidence. We have also studied the focusing ability of shallow and deep reflectors and demonstrated the splitting of the physical focus to two bright spots in the E-plane for reflectors deeper than $f/D = 0.25$.

ACKNOWLEDGMENT

The authors are grateful to Prof. G. Schettini and Prof. R. Sauleau for fruitful discussions.

REFERENCES

- [1] F. J. S. Moreira, A. Prata, and J. R. Bergmann, "GO shaping of omnidirectional dual-reflector antennas for a prescribed equi-phase aperture field distribution," *IEEE Trans. Antennas Propag.*, vol. 55, no. 1, pp. 99–106, 2007.
- [2] H.-T. Chou, P. H. Pathak, and R. J. Burkholder, "Application of Gaussian-ray basis functions for the rapid analysis of electromagnetic radiation from reflector antennas," *Proc. Inst. Electr. Eng. Microw., Antennas Propag.*, vol. 150, no. 3, pp. 177–183, 2003.
- [3] T. Bondo and S. B. Sorensen, "Physical optics analysis of beam waveguides using auxiliary planes," *IEEE Trans. Antennas Propag.*, vol. 53, no. 3, pp. 1062–1068, 2005.
- [4] S. M. Rao, D. R. Wilton, and A. W. Glisson, "Electromagnetic scattering by surfaces of arbitrary shape," *IEEE Trans. Antennas Propag.*, vol. 30, no. 3, pp. 409–418, 1982.
- [5] W. V. T. Rusch, "The current state of reflector antenna art," *IEEE Trans. Antennas Propag.*, vol. 32, no. 4, pp. 313–329, 1984.
- [6] A. G. Davydov, E. V. Zakharov, and Y. V. Pimenov, "Numerical solution method of the problem of electromagnetic wave diffraction by unclosed surface," *Sov. Phys. Dokl.*, vol. 276, no. 1, pp. 96–100, 1984.
- [7] D. C. Jenn, J. E. Fletcher, and A. Prata, "Radar cross section of symmetric parabolic reflectors with cavity-backed dipole feed," *IEEE Trans. Antennas Propag.*, vol. 41, no. 7, pp. 992–994, 1993.
- [8] A. Heldring, J. M. Rius, L. P. Ligthart, and A. Cardama, "Accurate numerical modeling of the TARA reflector system," *IEEE Trans. Antennas Propag.*, vol. 52, no. 7, pp. 1758–1766, 2004.
- [9] A. I. Nosich, "Method of Analytical Regularization in wave-scattering and eigenvalue problems: Foundations and review of solutions," *IEEE Antennas Propag. Mag.*, vol. 42, no. 3, pp. 34–49, 1999.
- [10] K. E. Warnik and W. C. Chew, "Error analysis of the moment method," *IEEE Antennas Propag. Mag.*, vol. 46, no. 6, pp. 38–53, 2004.
- [11] A. A. Nosich, Y. V. Gandel, T. Magath, and A. Altintas, "Numerical analysis and synthesis of 2-D quasioptical reflectors and beam waveguides based on an integral-equation approach and Nystrom's discretization," *J. Opt. Soc. Amer. A.*, vol. 24, no. 9, pp. 2831–2836, 2007.
- [12] J. L. Tsalamengas, "Exponentially converging Nystrom methods in scattering from infinite curved smooth strips. Part 1: TM-case," *IEEE Trans. Antennas Propag.*, vol. 58, no. 10, pt. 2, pp. 3275–3273, 2010.
- [13] Y. V. Gandel, *Introduction to the Methods of Computation of Singular and Hypersingular Integrals* (in Russian). Kharkiv: KhNU Press, 2001.
- [14] Y. V. Gandel and A. S. Kononenko, "Justification of the numerical solution of a hypersingular integral equation," *Differential Equations*, vol. 42, no. 9, pp. 1326–1333, 2006.
- [15] L. F. Canino, J. J. Ottusch, M. A. Stalzer, J. L. Visher, and S. M. Wandzura, "Numerical solution of the Helmholtz equation in 2D and 3D using a high-order Nyström discretization," *J. Comput. Phys.*, vol. 146, no. 2, pp. 627–663, 1998.
- [16] S. D. Gedney, "On deriving a locally corrected Nyström scheme from a quadrature sampled moment method," *IEEE Trans. Antennas Propag.*, vol. 51, no. 9, pp. 2402–2412, 2003.
- [17] S. D. Gedney, A. Zhu, and C. C. Lu, "Study of mixed-order basis functions for the locally-corrected Nyström method," *IEEE Trans. Antennas Propag.*, vol. 52, no. 11, pp. 2996–3004, 2004.
- [18] J. Strain, "Locally corrected multidimensional quadrature-rules for singular functions," *SIAM J. Sci. Comput.*, vol. 16, no. 4, pp. 992–1017, 1995.
- [19] M. G. Andreasen, "Scattering from bodies of revolution," *IEEE Trans. Antennas Propag.*, vol. 13, no. 2, pp. 303–310, Mar. 1965.
- [20] R. D. Graglia, P. L. E. Uslenghi, R. Vitiello, and U. D'Elia, "Electromagnetic scattering for oblique incidence on impedance bodies of revolution," *IEEE Trans. Antennas Propag.*, vol. 43, pp. 11–26, Jan. 1995.
- [21] M. R. Barclay and W. V. T. Rusch, "Moment-method analysis of large, axially symmetric reflector antennas using entire-domain functions," *IEEE Trans. Antennas Propag.*, vol. 39, no. 4, pp. 491–496, 1991.
- [22] A. Berthon and R. Bills, "Integral equation analysis of radiating structures of revolution," *IEEE Trans. Antennas Propag.*, vol. 37, no. 3, pp. 159–170, 1989.
- [23] A. G. Davydov, E. V. Zakharov, and Y. V. Pimenov, "Numerical analysis of fields in the case of electromagnetic excitation of unclosed surfaces," *J. Commun. Technol. Electron.*, vol. 45, no. 1.2, pp. 247–259, 2000.
- [24] A. V. Lugovoy and V. G. Sologub, "Scattering of electromagnetic waves by a disk at the interface between two media," *Sov. Phys. Tech. Phys.*, vol. 18, no. 3, pp. 427–429, 1973.
- [25] L. A. Pazynin and V. G. Sologub, "Diffraction radiation of a point charge moving along the axis of a segment of a circular waveguide," *Radiophys. Quantum Electron.*, vol. 27, no. 10, pp. 916–922, 1984.
- [26] S. S. Vinogradov, "Reflectivity of spherical shield," *Radiophys. Quantum Electron.*, vol. 26, no. 1, pp. 78–88, 1983.
- [27] D. B. Kuryliak and Z. T. Nazarchuk, "Illumination of a finite cone by an axial-symmetric electromagnetic wave," (in Russian) *Radio Phys. Radio Astron.*, no. 5, pp. 29–37, 2000.
- [28] E. N. Vasilyev, *Excitation of Bodies of Rotation* (in Russian). Moscow, Russia: Radio i Svyaz, 1987.
- [29] S. Skokic, E. Martini, and S. Maci, "Radar-invisibility on axis of rotationally symmetric reflectors," *IEEE Antennas Wireless Propag. Lett.*, vol. 4, no. 1, pp. 1–4, 2005.
- [30] P. Varga and P. Torok, "Focusing of electromagnetic waves by paraboloidal mirrors. Pt. I: Theory," *J. Opt. Soc. Amer. A.*, vol. 17, no. 11, pp. 2081–2089, 2000.
- [31] J. L. Tsalamengas, "Exponentially converging Nystrom methods in scattering from infinite curved smooth strips. Part 2: TH-case," *IEEE Trans. Antennas Propag.*, pp. 3274–3281.
- [32] P. Varga and P. Torok, "Focusing of electromagnetic waves by paraboloidal mirrors. Part II: Numerical results," *J. Opt. Soc. Amer. A.*, pp. 2090–2095.



Vitaliy S. Bulygin (M'09) was born in 1985 in Kharkiv, Ukraine. He received the M.S. degree in mathematical modeling from Kharkiv National University, in 2007 and the Ph.D. degree in mathematical modeling from the Institute of Problems of Machine Engineering, National Academy of Science of Ukraine (NASU), in 2010.

Since 2010, he has been with the Institute of Radio Physics and Electronics NASU, Kharkiv. His research interests are in integral equations, numerical methods, antennas, and electromagnetic

wave diffraction.

Dr. Bulygin won the N. I. Akhizezer Fellowship in 2009 and the Best Young Scientist Paper Prize of the European Microwave Association at MSMW-10 International Symposium, Kharkiv, in 2010.



Alexander I. Nosich (M'94–SM'95–F'04) was born in 1953 in Kharkiv, Ukraine. He received the M.S., Ph.D., and D.Sc. degrees in radio physics from the Kharkiv National University, Ukraine, in 1975, 1979, and 1990, respectively.

Since 1979, he has been with the Institute of Radio Physics and Electronics of the National Academy of Science of Ukraine, Kharkiv, where he is currently Professor and Principal Scientist heading the Laboratory of Micro and Nano-Optics. Since 1992, he has held a number of guest fellowships and professor-

ships in the EU, Japan, Singapore, and Turkey. His research interests include the method of analytical regularization, propagation and scattering of waves, open waveguides, antennas and lasers, and the history of microwaves

Prof. Nosich was one of the initiators and Technical Committee Chairman of the International Conference Series on Mathematical Methods in Electromagnetic Theory (MMET). In 1995, he organized IEEE AP-S East Ukraine Chapter, the first one in the former USSR. Currently he represents Ukraine, Georgia, and Moldova in the European Association on Antennas and Propagation



Yuriy V. Gandel (M'02–SM'04) was born in Kharkiv, Ukraine, in 1934. He received the M.S. and Ph.D. degrees in mathematical physics and the D.Sc. degree in radio physics from the Kharkiv National University, in 1962, 1971 and 1994, respectively.

Since 1995, he has been a Professor of mathematical physics at the Kharkiv National University. His research interests are in singular and hypersingular integral equations, numerical methods, and modeling of electromagnetic and acoustic wave scattering by screens and gratings.

Dr. Gandel was awarded the Honorary Medals of "Distinguished Teacher of Ukraine" and "Distinguished Educator of Ukraine" in 1967 and 2005, respectively, and an N. I. Akhizezer Fellowship in 2005. He was the co-recipient the Best Paper Award of the ISAP'04 International Symposium in Sendai, Japan, in 2004.